Entanglement of photons with complex spatial structure in Hermite-Laguerre-Gaussian modes

Jie Tang, Yang Ming,* Zhao-xian Chen, Wei Hu, Fei Xu, and Yan-qing Lu†

National Laboratory of Solid State Microstructures, College of Engineering and Applied Sciences, Collaborative Innovation Center of Advanced Microstructures, Nanjing University, Nanjing 210093, People's Republic of China

(Received 13 January 2016; published 7 July 2016)

Photons with complicated spatial mode structures can be applied for different quantum information tasks. Here, we show the entanglement of photons with complex singularity patterns called Hermite-Laguerre-Gaussian (HLG) modes. Measuring one photon of the entangled pairs by HLG mode basis to define its singularity pattern, we can steer the singularity structure of its partner, while the initial singularity structure of the photons is undefined. We also calculate the HLG specific quantum-correlation function. It can be used to extend the quantum key distribution protocols and to tune experiments dealing with high-order transverse modes. In addition we discuss orbital angular momentum properties of the HLG modes and summarize some features of the singularity pattern of the HLG modes with varying angle parameter.

DOI: 10.1103/PhysRevA.94.012313

I. INTRODUCTION

Quantum entanglement plays an important role in the fundamentals of quantum mechanics [1]. It is also widely used in the area of quantum information, for example, in quantum teleportation [2], quantum computation, and quantum cryptography [3]. Photon pairs may entangle in various degrees of freedom, such as polarization [4,5], time and energy [6], frequency [7], path [8], and transverse mode [9,10]. Additionally, entanglement of photons also extends to spatial modes of the electromagnetic field carrying orbital angular momentum (OAM) [11,12], which can be used to define an infinitely dimensional discrete Hilbert space and provide a practical route to entanglement that involves many orthogonal quantum states, instead of only two-dimensional entangled states. These entangled states with OAM make communication channels in quantum information more efficient and observably increase the transmission capacity [13].

The Laguerre-Gauss (LG) modes are a series of spatial modes carrying an OAM and have attracted much attention in several theories and experiments, such as two-dimensional entanglement of large quanta of OAM [14], multidimensional entanglement and cryptography [15], and entanglement of three-dimensional structures or quantum communication in free space [16]. The mode $\mathrm{LG}_{p,l}$ depends on two mode numbers, p and l. p is the number of radial nodes in the intensity distribution, which means the beam comprises $p+1$ concentric rings with a zero on-axis intensity in the intensity cross section, and l is the azimuthal index meaning that each photon carries an OAM of $l\hbar$ [17]. l is also called the topological charge of the phase singularities, and measures the strength of a net change of phase in a circuit enclosing the vortex. For LG modes with azimuthal index l, it seems that all singularities "merge" into a single isolated (l-fold degenerate) optical null at the center of the vortex [18].

Here, we concentrate on spatial modes that have more complex vortex distribution and singularity patterns called the Hermite-Laguerre-Gaussian (HLG) modes [19], which are a structurally stable solution of the paraxial wave equation as well. They have an additional continuous angle parameter α and each value defines a different set of orthonormal basis. The Hermite-Gauss (HG) modes emerge as a special case for $\alpha = 0$, and LG modes emerge when $\alpha = \pi/4$. Starting with LG modes as a special condition of HLG modes, when the angle parameter varies, it is accompanied by the splitting of merged singularities into l separate ones with unit topological charge, which constructs the specific phase and the intensity patterns. By changing the angle parameter and topological charge (the difference between two transverse mode numbers), the spatial distribution and the number of phase singularities can be well controlled [20]. In the famous EPR gedanken experiment, for a two-particle entangled state [21], the measurement of an observable of either particle determines the value of that observable for the other particle with unit probability. Here, we present an investigation with HLG modes in the quantum entanglement regime. In our discussion, a measurement of a specific singularity pattern on one photon defines the singularity pattern of the other one distantly, which implies the nonlocality involved in the operation. As HLG modes carry a fractional value of OAM, quantum-correlation properties of different angular momentum states with fractional values are also discussed.

In the following section, we briefly introduce the HLG modes and review some results on the correlation among general transverse modes of the pump, signal, and idler photon. Then, we simulate the coincidence counts rate between two first-order HLG modes and two high-order HLG modes, respectively, to reveal the entanglement properties involved in these modes with complex singularity patterns. We also calculate the correlation function between biphotons projected on high-order HLG modes with the same transverse mode number but a different angle parameter α. Steering by this angle parameter might be useful in quantum information protocols. In addition, we focus on the nonclassical OAM properties of the HLG modes and discuss the distinction conservation law of OAM between integral and fractional conditions. Finally,

*njumingyang@gmail.com
†yqlu@nju.edu.cn

we summarize some features of the singularity pattern of HLG modes on varying the angle parameter for completeness.

II. HERMITE-LAGUERRE-GAUSSIAN MODES

It is well known that beam families such as HG beams or LG beams play an important role in resonators and optical waveguides. As a structurally stable solution of the paraxial wave equation, each of them is the basis for the space $L_2(\mathbb{R}^2)$ (two-dimensional plane), and thus can be transformed mutually [22]. In 2004, Abramochkin proposed a unity of HG and LG beam families by introducing an additional parameter that keeps many properties of both families; these were called the Hermite-Laguerre-Gaussian modes.

Using the Cartesian coordinate system and assuming the z axis to be the propagation axis, the HLG beam in the $z = 0$ plane can be expressed as [19]

$$G_{n,m}(x,y|\alpha) = \exp(-x^2-y^2)\sum_{k=0}^{n+m} i^k \cos^{n-k}\alpha \sin^{m-k}\alpha \times P_k^{(n-k,m-k)}[-\cos(2\alpha)] H_{n+m-k}(\sqrt{2}x) H_k(\sqrt{2}y), \quad (1)$$

where $P_k^{(\mu,\nu)}(t)$ is the Jacobi polynomial and $H_n(x) = (-1)^n e^{x^2}\frac{d^n}{dx^n}e^{-x^2}$ is the nth-order Hermite polynomial. n and m are the transverse mode numbers in the x and y direction, respectively. α is the introduced angle parameter which allows a continuous transformation between HG modes and LG modes, and considering the periodicity, its value is often taken to be from 0 to 2π. For any fixed α, m and n can take any integer, and they belong to a new family that is also an orthogonal basis of the space $L_2(\mathbb{R}^2)$, and they thus define an infinite-dimensional Hilbert space. When α is equal to 0, the HLG beam reduces to a HG beam. When α is equal to $\pi/4$, the HLG beam transforms to a LG beam. It is seen that

$$G(x,y|0) = (-i)^m H_{n,m}(x,y), \quad (2)$$

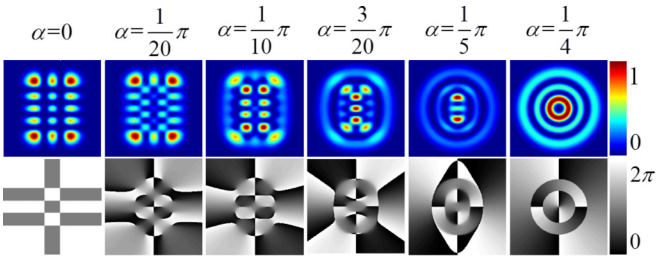

FIG. 1. Hermite-Laguerre-Gaussian mode $G_{4,2}(x,y|\alpha)$ with varying angle parameter, where $\alpha \in [0,\pi/4]$. The intensity (or phase) distribution of each mode is shown in the upper (or lower) row. From left to right, the values of α are an arithmetic progression. From right to left, the splitting of the central phase singularity on a horizontal line can be observed as well as the creation of additional pairs of singularities in the ring of zero intensity. For $\alpha = 0$, the HLG mode becomes the HG mode, which remains only a rectangular symmetry; for $\alpha = \pi/4$, the HLG mode becomes the LG mode, which has a rotational symmetry.

and

$$G_{n,m}\left(x,y\middle|\frac{\pi}{4}\right) = \begin{cases}(-1)^m 2^n m! L_{m,n-m}(x,y) & (n \geqslant m)\\ (-1)^n 2^m n! L_{n,m-n}(x,-y) & (n \leqslant m)\end{cases}. \quad (3)$$

This transition can be seen in Fig. 1.

III. TWO-DIMENSIONAL ENTANGLEMENT AND QUANTUM-CORRELATION FUNCTION

A. Parametric process

We still employ spontaneous parametric downconversion (SPDC) in a nonlinear crystal to generate entangled photon pairs. A typical material considered here is periodically poled lithium niobate (PPLN), where the quasi-phase-matching (QPM) technique is applied through suitable modulation of nonlinear susceptibility to get high conversion efficiency [23,24]. Using its largest nonlinear coefficient d_{33}, the two downconverted photons have different frequencies and we can split them with a dichroic mirror. We treat the pump wave classically and use the approximation that the amplitude is spatially constant. Based on the rotating wave approximation, we obtain H_{SPDC} as

$$H_{\mathrm{SPDC}} = -\frac{\hbar d_{33} E_p}{2}\iint d\omega_s d\omega_i \left[G_1 h(L\Delta\vec{k})\sqrt{\frac{\omega_s\omega_i}{n_s^2 n_i^2 N_s N_i}} \times F a_s^\dagger a_i^\dagger e^{-i(\omega_p-\omega_s-\omega_i)t} + \mathrm{H.c.}\right], \quad (4)$$

where $\Delta\vec{k}=\vec{k}_p-\vec{k}_s-\vec{k}_i-2\pi/\Lambda$ is the phase mismatch for the first-order QPM and G_1 is a corresponding Fourier coefficient, and Λ is the period of the QPM structure in the propagation direction. N_s, N_i are normalization parameters and n_s, n_s are the refractive indices. E_p is determined by the pump field. The value of $h(L\Delta\vec{k})$ is from the function of the form $h(x) = \exp(-ix/2)\sin c(x/2)$. $F = \iint d^2\vec{r}\,\Phi_p\Phi_s^*\Phi_i^*$ is the overlap integral of the normalized transverse mode profiles. Starting from a vacuum input, the two-photon state is derived as

$$|\psi\rangle = -\frac{i}{\hbar}\int_{-\infty}^{\infty} dt\, H_{\mathrm{SPDC}}(t)|0\rangle = \int d\nu \Gamma F a_s^\dagger a_i^\dagger|0\rangle, \quad (5)$$

where $\Gamma = (id_{33}E_p/2)G_1 h(L\Delta\vec{k})\sqrt{\omega_s\omega_i/n_s^2 n_i^2 N_s N_i}$. The frequency integration based on ω_i could be eliminated due to the temporal integration $\int \exp[-i(\omega_p-\omega_s-\omega_i)t] = \delta(\omega_p-\omega_s-\omega_i)$. Here we set $\omega_s = \Omega_s + \nu$, in which Ω_s is the perfect phase-matching frequency, and ν is the natural bandwidth.

As we are concerned with the transverse mode correlation implied in the overlap integral F, it is reasonable to assume that the conditions imposed by the nonlinear susceptibility and the QPM condition in Γ are always satisfied. Moreover, we ignore the influence due to the bandwidth of photons. Therefore, the two-photon state in the position representation takes the

form [25]

$$|\psi\rangle = \int d\vec{x}_s \int d\vec{x}_i \Phi_p\left(\frac{\vec{x}_s + \vec{x}_i}{2}\right)\Delta(\vec{x}_s - \vec{x}_i)\hat{a}_s^\dagger(\vec{x}_s)\hat{a}_i^\dagger(\vec{x}_i)|0\rangle. \tag{6}$$

The count rates of coincidence measurements are proportional to the probabilities of detecting a photon of the signal or idler in a specific mode, which can be calculated through projection operation of state vectors. Then, the normalized coincidence probability is given by

$$P_N(\Phi_i, \Phi_s) = \frac{\left|\int d\vec{X}\Phi_i^*(\vec{X})\Phi_s^*(\vec{X})\Phi_p(\vec{X})\right|^2}{\sqrt{\int d\vec{X}|\Phi_i^*(\vec{X})\Phi_p(\vec{X})|^2}\sqrt{\int d\vec{X}|\Phi_s^*(\vec{X})\Phi_p(\vec{X})|^2}}. \tag{7}$$

The probability becomes 1 if the signal and idler are perfectly correlated, and vanishes if the signal and idler are anticorrelated. For other conditions, it takes values between 0 and 1. Moreover, the state of the idler photon collapses into $|\psi_i\rangle = \langle\psi_s\,|\,\psi\rangle$ if we detect the biphoton state with a signal photon in the mode $|\psi_s\rangle$; thus the mode function of the idler can be expressed as

$$\Phi_2 = C\Phi_0\Phi_1^*. \tag{8}$$

The factor C ensures the normalization of the idler mode. These relationships are valid for any transverse mode function. In the next section, we concentrate on the HLG mode basis states by substituting mode function with specific transverse mode number and angle parameter.

B. Two-dimensional entanglement of the first-order HLG modes

In our designed scheme (Fig. 2), SPDC in the PPLN is employed to generate a biphoton, which has been discussed in the previous section. We split the photons with a dichroic beam splitter (DBS). In the two arms of the light path, a combination of spatial light modulators (SLMs) and single-mode fibers plays the role of a specific-mode spatial filter. Using computer-generated holograms, specific diffraction patterns load on the SLMs, which allows a desired high-order mode photon to convert into a Gaussian mode and couple into a single mode fiber (SMF). Then, avalanche photodiodes collect the delivered photons and a coincidence count takes place.

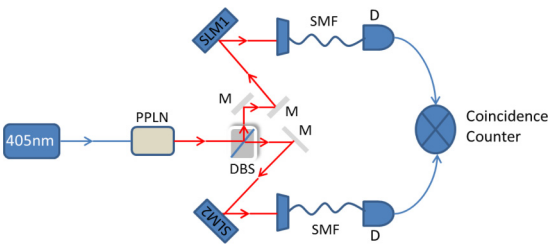

FIG. 2. Sketch of designed scheme. A PPLN crystal is employed to generate entangled photon pairs. We separate the biphoton with a dichroic beam splitter and convert the HLG mode into a Gaussian mode by SLMs. Then, the photons are coupled into SMFs and detected with avalanche photodiodes.

We first analyze the first-order HLG modes. It is known that any state of complete polarization can be described as a point on the Bloch sphere for the polarization, which is represented as a superposition of left- and right-handed circular polarizations. As an analogy to this, the same geometrical approach can be applied to construct a Bloch sphere for the representation of states within any two-dimensional subspace [26,27], with two basis elements $LG_{0,1}$ and $LG_{0,-1}$ at the poles, respectively. All the stable beam modes of order 1 can be represented as the superposition of $LG_{0,1}$ and $LG_{0,-1}$; thus, there is a one-to-one correspondence between every point on this Bloch sphere and every mode of order 1. In general terms, a state $|\vec{a}\rangle$ can be written as

$$|\vec{a}\rangle = \cos\left(\frac{\theta_a}{2}\right)|l\rangle + e^{i\phi_a}\sin\left(\frac{\theta_a}{2}\right)|-l\rangle, \tag{9}$$

where $\vec{a}$ is a vector pointing to a specific first-order mode. θ_a and ϕ_a are the polar angle and the azimuthal angle, respectively. The order of HLG modes is $N = n + m$, which is independent of the angle value α. The Bloch sphere gives a visual representation of first-order HLG modes with different values of α. When a left-handed circularly polarized light is transformed to a linear polarization with a quarter-wave plate, it can be represented by a move from the north pole to a point on the equator, the azimuthal angle of which depends on the orientation of the linear polarization. When representing states on the Bloch sphere, the cylindrical lens mode converters transform the transverse modes in a similar way as the wave plates transform the polarization state represented on the Bloch sphere for the polarization. Additionally, recalling that HLG modes can be obtained from the conversion between LG and HG modes, we finally conclude that the first-order HLG modes with different values of α can be represented around a closed longitude on the Bloch sphere. The azimuthal angle of the longitude depends on the position of the corresponding HG mode on the equator when α is equal to $\pi/2$. To be precise, for the $G_{1,0}(x,y|\alpha)$ mode [Fig. 3(a)], the connection between coordinate parameters and angle parameters is given as follows:

$$\begin{aligned} \phi_a &= 0, \\ \alpha &= \frac{3}{4}\pi - \frac{\theta_a}{2}(0 \leqslant \theta_a \leqslant 2\pi). \end{aligned} \tag{10}$$

As a specific example, we analyze the condition when the pump is a Gaussian mode, and the signal and idler are $G_{1,0}(x,y|\alpha)$ and $G_{1,0}(x,y|\beta)$ modes, respectively. On both SLMs we load the relevant phase pattern for the state at the longitude of the Bloch sphere, which corresponds to first-order HLG modes. We can fix the angle parameter α of the pattern on SLM1, and scan through the pattern from $\beta = \frac{\pi}{4}$ to $\beta = \frac{3\pi}{4}$ on SLM2. The simulative coincidence counts rate can be represented as a function of both parameter α and β as

$$P_N \propto \cos^2(\beta + \alpha). \tag{11}$$

For a specific signal mode, the coincidence counts rate varies as $\sin^2\theta$ function with the angle parameter of the idler mode. We observe nonclassical biphoton fringes with high visibility in Fig. 3(b). As a result, for a specific value of α, the state

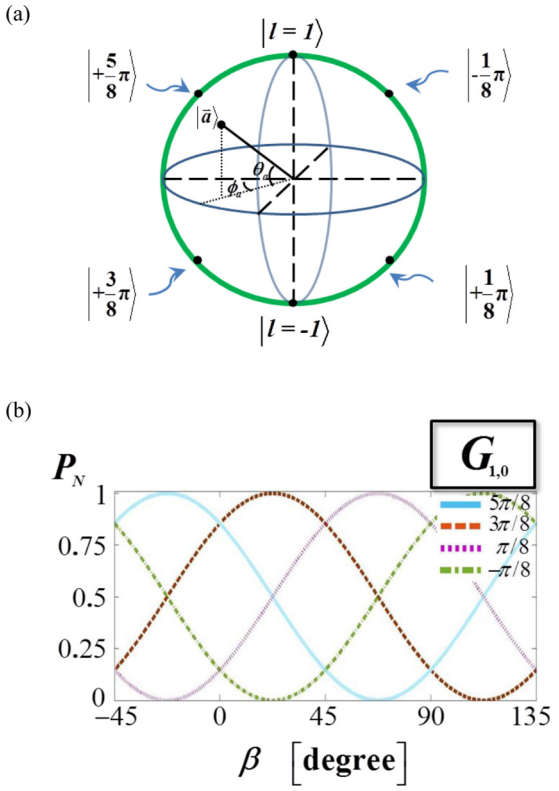

FIG. 3. (a) Bloch sphere representation of specific first-order HLG modes with different angle parameter. With the angle parameter changing continuously, the corresponding points move around a closed longitude. (b) Coincidence fringes for $G_{1,0}(x,y|\alpha)$, with four different angle parameter settings for the signal modes ($\frac{5}{8}\pi$, $\frac{3}{8}\pi$, $\frac{1}{8}\pi$, and $-\frac{1}{8}\pi$, respectively) and idler modes scanning from $-\frac{1}{4}\pi$ to $\frac{3}{4}\pi$.

after post-selection resembles a Bell state $|\psi^+\rangle$ in the form

$$|\Psi^{\alpha}\rangle=\frac{1}{\sqrt{2}}(|+\alpha\rangle_s|-\alpha\rangle_i+|-\alpha\rangle_s|+\alpha\rangle_i), \tag{12}$$

where the state vector $|\pm\alpha\rangle$ represents a photon in the first-order HLG mode $G_{1,0}(x,y|\pm\alpha)$. In fact, when we apply Eq. (8) to the condition when the pump is Gaussian mode and the signal is $G_{1,0}(x,y|\alpha)$ mode, the idler mode has the form (Fig. 4)

$$G_{1,0}(\sqrt{2}x,\sqrt{2}y|-\alpha)=G_{0,0}(x,y)G^{*}_{1,0}(x,y|\alpha). \tag{13}$$

The idler mode has the same transverse mode numbers as the signal mode, while the sign of the angle parameter is opposite, which gives rise to the results in Fig. 3(b). It is also seen that the scale of the idler light field reduces to $1/\sqrt{2}$ with respect to the pump and signal.

For HLG modes of order $N\geqslant 2$, there is no Poincaré-sphere equivalent; we can still restrict ourselves to two-dimensional subspace by defining a Bloch sphere in another form given as [18]

$$G^{\theta,\phi}_{n,m}(x,y)=\cos\theta\exp(i\phi)\mathrm{G}_{n,m}\left(x,y\middle|\frac{\pi}{4}\right)+\sin\theta\exp(-i\phi)G_{n,m}\left(x,y|-\frac{\pi}{4}\right), \tag{14}$$

where θ goes from 0 to $\pi/2$ and ϕ goes from 0 to π. Similarly, the poles are LG modes when the angle parameter of the corresponding HLG modes is set to particular values. In the first-order condition, an arbitrary closed longitude on the Bloch sphere corresponds to the HLG modes of the same order or their superposition, but for high-order conditions, only a few specific points on the closed longitude correspond. Any other points must be represented in a superposition of different-order HLG modes due to the limited dimension of the Bloch sphere.

As a specific example, we analyze points on the equator, which represent a superposition of poles with the same weight but different phase ϕ. In Fig. 5(a), the sphere of the mode $G^{\theta,\phi}_{4,2}(x,y)$ is shown, for which the HLG mode elements are shown in Fig. 1. On the equator, the hologram for four specific phases is chosen to be displayed on SLM1, while the SLM2 scans around the equator. The normalized coincidence counts rate is shown as a function of the phase [in Fig. 5(b)], which fits the $\sin^2\theta$ curve. We observe once again the nonclassical biphoton fringes with high visibility and expect the two-dimensional entanglement state in the form

$$|\Psi^{\phi}\rangle=\frac{1}{\sqrt{2}}(|\phi_1\rangle_s|\phi_2\rangle_i+|\phi_2\rangle_s|\phi_1\rangle_i), \tag{15}$$

where $|\phi_j\rangle(j=1,2)$ represents a state on the equator in the mode $G^{\pi/4,\phi_j}_{4,2}(x,y)$. For other high-order HLG modes, we can get the same coincidence fringes.

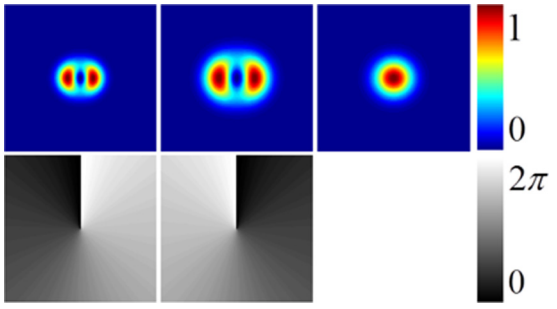

FIG. 4. Intensity (upper row) and phase (lower row) patterns of the idler beam (left column) with the signal beam in mode $G_{1,0}(x,y|\pi/3)$ (middle column) and pump beam in a Gaussian mode (right column).

C. Quantum-correlation function of the HLG modes

Selecting the HLG modes as a basis for the space $L_2(\mathbb{R}^2)$, the downconverted biphoton with arbitrary transverse mode function can be considered in a superposition state of HLG modes elements with a different transverse mode number and angle parameter. Therefore, we analyze the correlation between the two downconverted photons when they are projected onto certain HLG modes elements. As the HLG beam can be expressed in terms of the LG modes, a unitary transformation relates the LG mode basis to the HLG mode basis. This unitary transformation can be understood as a rotation transformation. Then, the angle parameter α is the characteristic rotation parameter, and the HLG modes are treated as a rotated basis with respect to the LG modes. In

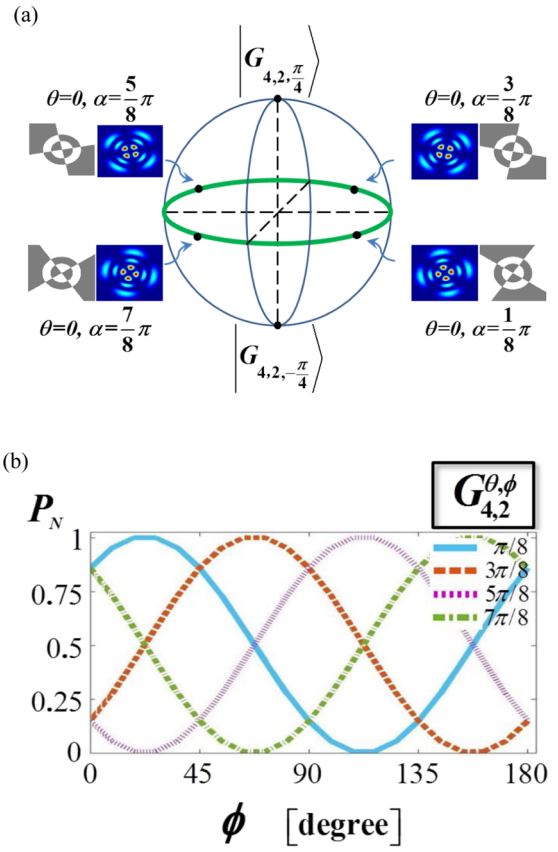

FIG. 5. (a) Redefined Bloch sphere representation of high-order HLG modes $G^{\theta,\phi}_{4,2}(x,y)$.The insets show the intensity (left) and phase patterns (right) of four chosen signal modes. (b) Coincidence fringes for $G^{\theta,\phi}_{4,2}(x,y)$ on the equator, with four different phase value settings for the signal modes ($\frac{1}{8}\pi$, $\frac{3}{8}\pi$, $\frac{5}{8}\pi$, and $\frac{7}{8}\pi$) and idler modes scanning from 0 to π.

addition to the specific example of $G_{1,0}(x,y|\alpha)$ discussed in the previous section, we calculate several sets of overlap integrals between the two HLG modes with the same values of n and m, but different values of α for measuring the correlation between the two rotated basis elements (Fig. 6). To implement this measurement, we display on SLM1 and SLM2 with phase patterns of the corresponding HLG modes, and measure the coincidence count rate when α is varied and all other parameters fixed.

When the two values of α match, we can obtain the maximum coincidence rate, while for different values of α, the coincidence rate decreases. When the transverse mode number increases, the decrease of the coincidence rate resulting from the deviation between α also increases. This can be understood when we expand the HLG modes into the HG basis. The higher the order of the HLG modes, the more HG basis elements are involved and hence the expansion coefficient is smaller. As different HG basis elements are mutually orthogonal and have no contribution to the overlap integral, when the number of expansion terms is larger, smaller results can be obtained due to the relatively smaller value of the modulus square of all expansion coefficients.

The basis rotation performed by the parameter α affects the whole infinite-dimensional Hilbert space constructed using the HLG basis, and hence, a HLG mode with a specific α cannot be fully reconstructed by finite basis elements defined by a different value of α. As a result, when calculating the coincidence rate, we obtain the nonzero results, which are always less than 1. We can use this property to extend protocols for quantum key distribution, such as BB84 schemes [28] or two-step ones [29]. As an illustrative example, we would propose a preliminary two-step filter-based quantum key distribution (QKD) protocol, in which Alice transmits one-bit information to Bob in two steps. After the two steps, Bob performs measurement on the two parts and obtains the full one bit. The Z basis is defined by, e.g., $|0\rangle \equiv G_{1,0,\alpha}, |1\rangle \equiv G_{0,1,\alpha}$ and the X basis is defined by $|0\rangle \equiv \frac{1}{\sqrt{2}}(G_{1,0,\alpha} + G_{0,1,\alpha})$, $|1\rangle \equiv \frac{1}{\sqrt{2}}(G_{1,0,\alpha} - G_{0,1,\alpha})$. In the first step, Alice sends an arbitrary α from some previously designed ones, i.e., $\alpha = 0, \frac{\pi}{8}, \frac{\pi}{4}$, along one channel. In the second step, she chooses randomly from one of the four states with HLG modes dependent on the α transmitted in step 1 and sends it to Bob in another separated channel. After Bob receives the specific α and state transmitted in step 2, he performs a measurement on his HLG modes by randomly selecting a state from one of the four states determined by this specific α. After a sequence of this procedure, they can share a random bit string, which is the raw key.

Two channels should be separated to prevent possible eavesdropping. Eavesdropping on only one of the channels implies that the eavesdropper can never extract enough information of the basis which Alice and Bob are using. If two channels can be eavesdropped on at the same time, the time interval of transmitting α in step 1 should set to be random (and therefore unknown to Eve) while in step 2, the time interval is fixed. It does not affect Bob's choice of basis because he performs a measurement sequentially after

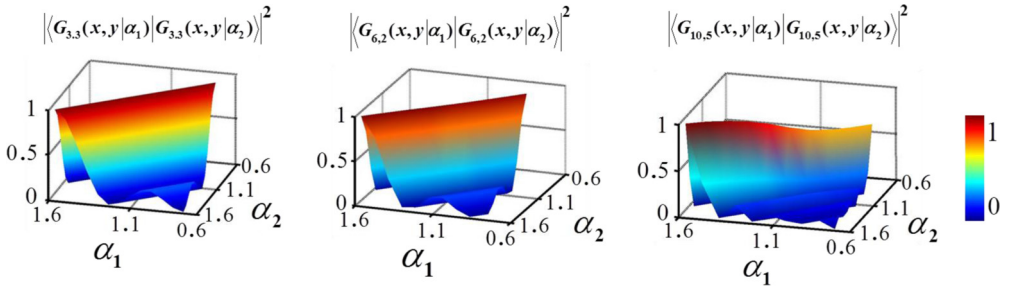

FIG. 6. Overlap integrals between HLG modes with the same transverse mode number but different angle parameter α. When the angle parameter is different, the overlap decreases. From left to right, the mode numbers (n, m) are (3, 3), (6, 2), and (10, 5), respectively.

receiving two full parts. For eavesdroppers, the random time delays between two steps break the correspondence of α and the computational basis and force them to face the additional task of getting the correct value of the α. Guessing a wrong value of α, the eavesdropper measures in the incorrect basis, and he will obtain less meaningful information but instead introduce a disturbance in the system, resulting in its detection. What is more, the information which the adversary needs to guess is up to the amount of the preset values of α in step 1. If in step 1, Alice chooses an α randomly from three previously designed ones per round, then each value of α will appear with the identical possibility. So the adversary needs to guess $\log_2 3$ extra bits of information per round compared with protocols without using α. In comparison to QKD protocols which manipulate OAM modes [30] or other transverse modes [31], encoding information in the HLG modes basis has the advantage of more security and flexibility.

IV. ANGULAR MOMENTUM PROPERTIES

Angular momentum of the HLG beams is another subject of interest. The OAM per photon in linearly polarized HLG modes is given by [18]

$$L[G_{n,m}(x,y|\alpha)] = \frac{n-m}{\omega}\sin 2\alpha. \tag{16}$$

It is seen that HG modes (e.g., $\alpha = \pi/2$) have no OAM, while the LG (e.g., $\alpha = \pi/4$) modes have OAM. For any fixed transverse mode number, when α varies in a continuous manner, the corresponding OAM values of the HLG beam are also continuous. They can be considered as suitable basis elements to tune fractional OAM [32]. Moreover, as a deduction of the overlap integral between different HLG mode functions mentioned in the previous section, the correlation of the OAM between the two downconverted photons mapping on a particular HLG mode basis is also obvious. The simulated results of the simplest example of this correlation between the first-order signal and idler HLG modes can be seen in Fig. 7(a).

We focus on whether or not the conservation of OAM can be fulfilled even for a fractional value condition. Actually, for a given pump mode, the signal and idler provide stronger correlation in two specific HLG modes because of the OAM conservation. Here, the OAM per photon is still defined as $l\hbar$, but l takes a fractional value as well. When the pump beam carries no OAM [e.g., Fig. 7(a), the pump is a Gaussian mode], the normalized coincidence rate becomes maximal if the OAM is conserved and vanishes when $|l_s - l_i| = 1$. Therefore, it is most likely to detect a pair of signal and idler modes that conserve the OAM of the pump beam, while it is impossible to find combinations of signal and idler modes that violate OAM conservation by one for first-order HLG mode. When the pump beam takes OAM [e.g., Fig. 7 (b)], a maximum of the normalized coincidence rate appears in the position where the integer OAM conserves. If we continue to detect higher-order modes, the coincidence rate is always found to be minimum whenever $|l_s - l_i|$ is equal to an integer, which represents the least possible detect combination. Note that there is a secondary maximum of the OAM correlation function in Fig. 7(b), and the coincidence rate in Fig. 7(a) decreases gradually in the direction perpendicular to the maximum line.

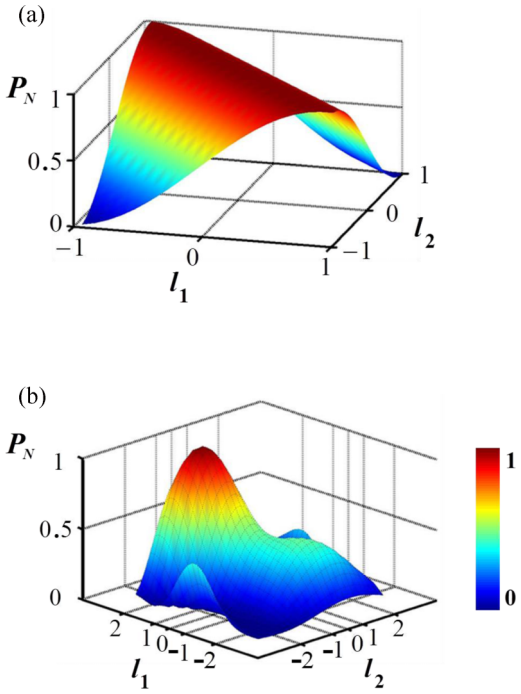

FIG. 7. (a) The correlation of the OAM between the signal and idler photons in the first-order HLG mode $G_{1,0}(x,y|\alpha)$ and the pump photon carrying no OAM. (b) The correlation of OAM between the signal and idler photons in the HLG mode $G_{2,0}(x,y)\infty$. The pump photon is in mode $G_{2,0}(x,y|\pi/12)$, which carries an OAM of $\hbar$ per photon. The maximum of the normalized coincidence rate appears in the position where the OAMs of the signal and the idler are $2\hbar$ and $-\hbar$, respectively.

These results seem to imply the violation of the conservation rule for the fractional OAM condition. However, it is not the case for this anomaly results from the method of calculating the coincidence rate. Because of the continuous value of α, the HLG mode basis is overcomplete and the modes with small deviation between α are not orthogonal. When we calculate the overlap integral between these two HLG modes, the additional quantity is inevitable, which gives rise to the nonzero results when the conservation condition is violated. Thus, the HLG modes with integer OAM satisfy the conservation rule strictly, while for the condition of fractional OAM, we can say that it is more likely to detect combinations of signal and idler modes, which conserve the OAM.

V. DISCUSSIONS

As mentioned above, with particular vortex and singularity patterns, the HLG modes have potential applications in quantum cryptography protocols, quantum imaging, and quantum pattern recognition. We firstly focus on the distribution of phase singularities (characteristic points with zero intensity) as the angle parameter α is varied. We calculate the intensity and phase of the HLG modes (Fig. 8) in the initial plane ($z = 0$) at a fixed value of n, m and at different values of α. It is seen to generate a column of isolated phase singularities on the y axis, in which the number is just the transverse mode number n. Note that for the case when $\alpha = 0$, the HLG beam is similar

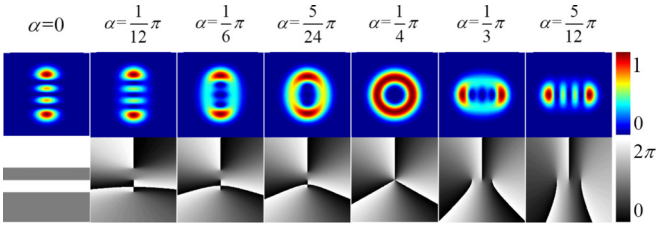

FIG. 8. Intensity (upper row) and phase (lower row) patterns of the HLG mode in the initial plane ($z = 0$) at fixed values of the transverse mode number ($n = 3, m = 0$) and different values of the angle parameter $0, \frac{1}{12}\pi, \frac{1}{6}\pi, \frac{5}{24}\pi, \frac{1}{4}\pi, \frac{1}{3}\pi, \frac{5}{12}\pi$.

to the standard $\mathrm{HG}_{n,0}$ mode, the phase singularities ceasing to be isolated, but rather the zero-intensity lines are parallel to the x axis. With the angle parameter increasing from 0 to $\pi/4$ when its absolute value is small, these isolated singularities converge slowly and maintain equal-interval distribution, but convert from lines to points quickly. However, as its absolute value increases, in particular when the value reaches $\pi/4$, the isolated singularities shift along the y axis toward the origin point, whereas at $\alpha = \pi/4$, all the singularities merge into a single isolated (n-fold degenerate) optical null at the origin, which is the main feature of the LG modes. The isolated singularities behave in a similar way along the x axis with the angle parameter varying from $\pi/4$ to $\pi/2$. In the phase patterns, each isolated singularity is associated with an optical vortex of topological charge -1 or $+1$. When the transverse mode number is larger, the "motion" of phase singularities becomes more complicated, generally in two steps. First, the equal-interval distributional isolated singularities tend to change their shape from line to point with positions essentially constant. Then, these singularities begin to converge towards the origin keeping the pointlike shape. The reason for the behavior of phase singularities may relate to the value of the polynomial's root of the mode expression, where further research is expected.

In Sec. III C, some potential applications of using HLG modes in QKD have been proposed. As we know, mutually unbiased bases (MUBs) are frequently used in drawing up efficient QKD protocols. Here we still use a linear combination of HLG modes to construct a mutually unbiased basis set, which is in analogy with the high-dimensional QKD with OAM. It is not evident that changing the α of the primary encoding basis merely can be employed to construct MUBs, though this looks like an exciting subject. Introducing the continuous α parameter may result in the nonorthogonality of wave functions and become a major obstacle in finding MUBs. However, the vanishing overlap in Fig. 6 indicates that orthogonal modes can appear by altering α, and what we should do is to find some appropriate values of α which maintain the orthogonality of the HLG modes according to practical needs. What is more, similar to the original BB84 protocol, we can also choose two different values of α, each of them defining a HLG modes basis. For any fixed α, modes $\{G_{n,m}(x,y|\alpha); n,m = 0,1,2\cdots\}$ in the same basis are orthogonal and modes in a different basis are nonorthogonal. With the convenience of manipulating HLG modes in the practical operation, we believe the applications of HLG modes in this field are very promising.

VI. CONCLUSIONS

In conclusion, we show the entanglement property of photons in the first-order HLG modes. Moreover, by redefining the Bloch sphere, the nonclassical correlation property of the high-order HLG modes with a specific singularity pattern structure is also discussed. We can use these properties to nonlocally steer the distribution of singularities on one photon by measuring the singularity pattern on another photon. We then calculate the overlap integral depending on the angle parameter for measuring the correlation between two specific HLG modes, which can be used to extend the quantum key distribution protocols and to tune experiments dealing with high-order transverse modes. In a perspective of angular momentum, the finite mode overlap between modes differing by fractional OAM reveals that the conservation law of OAM is distinct between the integral and fractional condition. For the latter case, it is most likely to detect combinations of the signal and idler modes, which conserve the OAM. The HLG modes with a continuous value of OAM provide a platform to investigate classical or nonclassical properties for angular momentum states with a fractional value. Finally, we summarize some features of the singularity pattern of the HLG modes with varying angle parameter.

ACKNOWLEDGMENTS

This work was supported by National 973 Program No. 2012CB921803; by the National Science Fund of China under Grants No. 61225026, No. 61435008, and No. 61490714; and by the Program for Changjiang Scholars and Innovative Research Team at the University under Contract No. IRT13021. We acknowledge Prof. Lijian Zhang for his kind help in revising the manuscript.

[1] D. Bouwmeester, A. Ekert, and A. Zeilinger,*The Physics of Quantum Information* (Springer-Verlag, Berlin, 2000).
[2] D. Bouwmeester, J. Pan, K. Mattle, M. Eibl, H. Weinfurter, and A. Zeilinger, Nature **390**, 575 (1997).
[3] N. Gisin, G. Ribordy, W. Tittel, and H. Zbinden, Rev. Mod. Phys. **74**, 145 (2002).
[4] S. J. Freedman and J. F. Clauser, Phys. Rev. Lett. **28**, 938 (1972).
[5] Y. Ming, A. H. Tan, Z. J. Wu, Z. X. Chen, F. Xu, and Y. Q. Lu, Sci. Rep. **4**, 4812 (2014).
[6] P. G. Kwiat, A. M. Steinberg, and R. Y. Chiao, Phys. Rev. A **47**, R2472 (1993).
[7] S. Ramelow, L. Ratschbacher, A. Fedrizzi, N. K. Langford, and A. Zeilinger, Phys. Rev. Lett. **103**, 253601 (2009).
[8] J. G. Rarity and P. R. Tapster, Phys. Rev. Lett. **64**, 2495 (1990).
[9] M. Krenn, R. Fickler, M. Huber, R. Lapkiewicz, W. Plick, S. Ramelow, and A. Zeilinger, Phys. Rev. A **87**, 012326 (2013).
[10] Y. Ming, Z. J. Wu, G. X. Cui, A. H. Tan, F. Xu, and Y. Q. Lu, Appl. Phys. Lett. **104**, 171110 (2014).

[11] A. Mair, A. Vaziri, G. Weihs, and A. Zeilinger, Nature **412**, 313 (2001).
[12] Y. Ming, J. Tang, Z. X. Chen, F. Xu, L. J. Zhang, and Y. Q. Lu, IEEE J. Sel. Top. Quantum Electron. **21**, 6601206 (2015).
[13] G. Molina-Terriza, A. Vaziri, J. Rehacek, Z. Hradil, and A. Zeilinger, Phys. Rev. Lett. **92**, 167903 (2004).
[14] R. Fickler, R. Lapkiewicz, W. N. Plick, M. Krenn, C. Schaeff, S. Ramelow, and A. Zeilinger, Science **338**, 640 (2012).
[15] M. Mirhosseini, O. S. Magaña-Loaiza, M. N. O'Sullivan, B. Rodenburg, M. Malik, M. P. J. Lavery, M. J. Padgett, D. J. Gauthier, and R.W. Boyd, New J. Phys. **17**, 033033 (2015).
[16] M. Malik, M. O'Sullivan, B. Rodenburg, M. Mirhosseini, J. Leach, M. P. J. Lavery, M. J. Padgett, and R.W. Boyd, Opt. Express **20**, 13195 (2012).
[17] L. Allen, M. W. Beijersbergen, R. J. C. Spreeuw, and J. P. Woerdman, Phys. Rev. A **45**, 8185 (1992).
[18] A. M. Yao and M. J. Padgett, Adv. Opt. Photonics **3**, 161 (2011).
[19] E. G. Abramochkin and V. G. Volostnikov, J. Opt. A: Pure Appl. Opt. **6**, S157 (2004).
[20] D. M. Deng and Q. Guo, Opt. Lett. **33**, 1225 (2008).
[21] A. Einstein, B. Podolsky, and N. Rosen, Phys. Rev. **47**, 777 (1935).
[22] I. Kimel and L. R. Elias, IEEE J. Quantum Electron. **29**, 2562 (1993).
[23] G. H. Shao, Z. J. Wu, J. H. Chen, F. Xu, and Y. Q. Lu, Phys. Rev. A **88**, 063827 (2013).
[24] T. Suhara and H. Kintaka, IEEE J. Quantum Electron. **41**, 1203 (2005).
[25] S. Franke-Arnold, S. M. Barnett, M. J. Padgett, and L. Allen, Phys. Rev. A **65**, 033823 (2002).
[26] M. J. Padgett and J. Courtial, Opt. Lett. **24**, 430 (1999).
[27] E. J. Galvez, P. R. Crawford, H. I. Sztul, M. J. Pysher, P. J. Haglin, and R. E. Williams, Phys. Rev. Lett. **90**, 203901 (2003).
[28] C. H. Bennett and G. Brassard, in *Proceedings of the IEEE International Conference on Computers, Systems, and Signal Processing* (IEEE, Bangalore, India, 1984), p. 175.
[29] F. G. Deng, G. L. Long, and X. S. Liu, Phys. Rev. A **68**, 042317 (2003).
[30] M. Mafu, A. Dudley, S. Goyal, D. Giovannini, M. McLaren, M. J. Padgett, T. Konrad, F. Petruccione, N. Lutkenhaus, and A. Forbes, Phys. Rev. A **88**, 032305 (2013).
[31] M. A. Luda, M. A. Larotonda, J. P. Paz, and C. T. Schmiegelow, Phys. Rev. A **89**, 042325 (2014).
[32] J. B. Gotte, S. Franke-Arnold, R. Zambrini, and S. Barnett, J. Mod. Opt. **54**, 1723 (2007).